Cancer Cell
Article

Genetic *p53* Deficiency Partially Rescues the Adrenocortical Dysplasia Phenotype at the Expense of Increased Tumorigenesis

Tobias Else,[1,*] Alessia Trovato,[1] Alex C. Kim,[1] Yipin Wu,[2] David O. Ferguson,[2] Rork D. Kuick,[3] Peter C. Lucas,[2] and Gary D. Hammer[1,*]
[1]Metabolism Endocrinology and Diabetes, Department of Internal Medicine
[2]Department of Pathology
[3]Biostatistics Core of the Cancer Center
University of Michigan Health System, Ann Arbor, MI 48109-2200, USA
*Correspondence: telse@umich.edu (T.E.), ghammer@umich.edu (G.D.H.)
DOI 10.1016/j.ccr.2009.04.011

SUMMARY

Telomere dysfunction and shortening induce chromosomal instability and tumorigenesis. In this study, we analyze the adrenocortical dysplasia (*acd*) mouse, harboring a mutation in *Tpp1/Acd*. Additional loss of *p53* dramatically rescues the *acd* phenotype in an organ-specific manner, including skin hyperpigmentation and adrenal morphology, but not germ cell atrophy. Survival to weaning age is significantly increased in $Acd^{acd/acd}$ $p53^{-/-}$ mice. On the contrary, $p53^{-/-}$ and $p53^{+/-}$ mice with the $Acd^{acd/acd}$ genotype show a decreased tumor-free survival, compared with $Acd^{+/+}$ mice. Tumors from $Acd^{acd/acd}$ $p53^{+/-}$ mice show a striking switch from the classic spectrum of $p53^{-/-}$ mice toward carcinomas. The *acd* mouse model provides further support for an in vivo role of telomere deprotection in tumorigenesis.

INTRODUCTION

Telomere dysfunction has been shown to interfere with tissue maintenance and to induce chromosomal rearrangements, which can provide the genetic basis for malignant transformation (Artandi, 2002; Blasco, 2005). Telomeres, the outer ends of chromosomes, consist of stretches of hexameric repeats. Over multiple cell cycles, telomeres are shortened as a result of the inability of the semiconservative DNA replication to completely synthesize the 3′ end of linear chromosomes, which is also known as the end-replication problem. In some tissues and cancers, this problem is overcome by the activity of telomerase, a ribonucleoprotein that adds telomeric repeats to the 3′ end of the leading strand (reviewed by Greider, 1996).

Normal telomeres are protected through a specialized DNA structure (T-loop) and a set of protein factors, termed the shelterin complex, which prevents the chromosome ends from causing activation of the DNA damage surveillance and repair machinery, as well as regulating telomerase access (de Lange, 2005). Although some parts of the shelterin complex directly bind to either double-stranded (TRF1 and TRF2) or single-stranded (POT1) telomere repeats, TIN2, RAP1, and TPP1/ACD serve as critical interconnectors of the shelterin complex. TPP1/ACD (originally termed PTOP, TINT1, and PIP1) was first described as an integral part of the shelterin complex that binds to POT1 and TIN2 (Houghtaling et al., 2004; Liu et al., 2004; Ye et al., 2004). We and others have since shown TPP1/Acd to be necessary for the recruitment of POT1 to the telomere and, moreover, that it is required for the telomere protective and length regulatory function of POT1 (Hockemeyer et al., 2007; Xin et al., 2007).

Concurrent with the cloning of human *TPP1/ACD*, we had identified a recessive mutation (Acd^{acd}) in the mouse ortholog of the gene encoding TPP1 as the genetic cause of the adrenocortical dysplasia (*acd*) phenotype, hence termed *Acd* (Keegan et al., 2005). The *acd* phenotype displays a significant overlap

SIGNIFICANCE

Critically shortened dysfunctional telomeres of the $Terc^{-/-}$ mice have been shown to impact tissue development and maintenance and lead to the occurrence of a procancer genome. The present study examines the contribution of telomere shortening versus telomere deprotection to the development of genetic instability and cancer. By studying the *acd* mouse, we show that telomere deprotection without significant telomere shortening is sufficient to induce tumor formation in the context of p53 absence. It also raises the possibility that telomere deprotection contributes to the high prevalence of carcinomas in humans.

with late-generation $Terc^{-/-}$ and $Tert^{-/-}$ mice (Lee et al., 1998; Liu et al., 2000; Rudolph et al., 1999). Both are infertile as the result of severely reduced spermatogenesis and have a reduced body size. In addition, the *acd* mouse is characterized by skin hyperpigmentation, patchy or absent fur growth, abnormal morphology of the adrenal cortex with large pleomorphic nuclei, skeletal abnormalities, and hydronephrosis (Beamer et al., 1994; Keegan et al., 2005).

Most of our current knowledge about the consequences of telomere dysfunction stems from analysis of the phenotype of the $Terc^{-/-}$ mouse, which lacks the telomerase RNA component. The phenotype of $Terc^{-/-}$ mice is believed to be due to a progressive shortening of telomeres over consecutive generations of $Terc^{-/-}$ homozygous breedings and over the lifetime of the $Terc^{-/-}$ organism (Blasco et al., 1997; Chin et al., 1999; Hande et al., 1999; Rudolph et al., 1999). With continued telomere shortening, cells from $Terc^{-/-}$ mice exhibit cytogenetic abnormalities, including chromosomal fusions, presumably due to the ligation of unprotected telomeres by the DNA repair machinery. Similar observations have been made in cell culture models of telomere deprotection, such as overexpression of a dominant negative isoform of TRF2 (van Steensel et al., 1998).

In contrast, the *acd* phenotype manifests within the first generation of $Acd^{acd/acd}$ mice generated by heterozygous matings (Beamer et al., 1994; Keegan et al., 2005). The telomere deprotection phenotype in cells lacking *TPP1/Acd* has been well described. The acute reduction of TPP1 levels in human cells induces telomere dysfunction-induced foci (TIFs) and telomere elongation (Guo et al., 2007; Hockemeyer et al., 2007; Liu et al., 2004; Ye et al., 2004). Mouse embryo fibroblasts (MEFs) from *acd* mice with a severe deficiency of Tpp1/Acd show a telomere deprotection phenotype and a moderate increase in genomic alterations, such as chromosome fusions (Else et al., 2007; Hockemeyer et al., 2007). The acute loss of Tpp1/Acd in *wt* MEFs strongly induces a DNA damage response, inducing senescence through a p53-sensitive pathway (Guo et al., 2007; Hockemeyer et al., 2007; Xin et al., 2007).

Telomere dysfunction of $Terc^{-/-}$ mice leads to the accumulation of genomic alterations and the development of tumors (Chin et al., 1999). Cells harboring critically short telomeres are usually removed from the pool of proliferating cells by p53-dependent pathways leading to apoptosis or senescence in mice and/or additional p16/Ink4a-sensitive pathways in humans (Jacobs and de Lange, 2004; Smogorzewska and de Lange, 2002). In accordance with this finding, $Terc^{-/-}$ $p53^{-/-}$ mice exhibit a partial reversal of their infertility as a result of germ cell failure at the expense of an increased tumor incidence (Artandi et al., 2000; Chin et al., 1999).

With the exception of the $Pot1b^{-/-}$ mouse, attempts to create deletions of components of the shelterin complex in whole murine organisms have led to phenotypes with early embryonic lethality (Celli and de Lange, 2005; Chiang et al., 2004; Hockemeyer et al., 2006; Karlseder et al., 2003; Wu et al., 2006). The $Acd^{acd/acd}$ genotype that results in a viable mouse, despite severe Tpp1/Acd deficiency, presents a unique opportunity to investigate the in vivo effects of direct telomere deprotection without telomere shortening (Else et al., 2007; Hockemeyer et al., 2007). To study the in vivo consequences of telomere dysfunction in the absence of telomere shortening, we crossed $Acd^{acd/acd}$ mice to a $p53^{-/-}$ background and analyzed the surviving offspring for both the rescue of organ phenotypes and the emergence of cancer.

RESULTS

Organ-Specific Rescue of the *acd* Phenotype by *p53* Ablation

Because the *acd* phenotype is predicted to be induced by telomere dysfunction, resulting in activation of p53-sensitive signaling pathways, we crossed $Acd^{acd/acd}$ mice to a $p53^{-/-}$ background. On macroscopic examination, a striking complete normalization of the characteristic *acd* phenotype of patchy or complete lack of fur and hyperpigmentation was evident in $Acd^{acd/acd}$ $p53^{-/-}$ mice (Figure 1A; see Figure S1A available online). Although the fur and skin phenotype of *acd* mice varied significantly between individual animals, hyperpigmentation in *acd* mice is always present in the skin overlying the paw pads, ears, tail, and the ano-genital region. In $Acd^{acd/acd}$ $p53^{-/-}$ mice, macroscopic hyperpigmentation was completely abolished, and there was a dramatic reduction of pigment in epidermis and dermis (Figure 1B; Figure S1B). Hyperpigmentation in *acd* mice not only led to a darker skin color but was also evident in skin-associated lymph nodes presumably because of the uptake and lymphatic transport by macrophages (Figure S2). These dark lymph nodes were not present in $Acd^{acd/acd}$ $p53^{-/-}$ mice (data not shown).

We analyzed the genotype of 162 male pups resulting from double heterozygous matings ($Acd^{+/acd}$ $p53^{+/-}$ × $Acd^{+/acd}$ $p53^{+/-}$) at weaning age (21 days). For $p53^{+/+}$ as well as $p53^{+/-}$ offspring, a significantly lower number of $Acd^{acd/acd}$ genotypes were observed than were expected ($p = 0.03$ and $p = 0.03$, χ^2 test), whereas for $p53^{-/-}$ offspring, the $Acd^{acd/acd}$ genotypes were nearly in the expected Mendelian proportions ($p = 0.6$), indicating that $p53^{-/-}$ increases survival of the $Acd^{acd/acd}$ genotype (Figure 1C). Like $Acd^{acd/acd}$ $p53^{+/+}$ mice, $Acd^{acd/acd}$ $p53^{-/-}$ mice were significantly smaller than their respective $Acd^{+/+}$ littermates at weaning age (3 weeks) and at 6 weeks of age ($p < 10^{-7}$) (Figure 1D).

Testes of both $Acd^{acd/acd}$ and late-generation $Terc^{-/-}$ mice, show similar germ cell failure (Hemann et al., 2001; Keegan et al., 2005; Lee et al., 1998). Therefore, we examined whether the observed spermatogenic defect involved p53 signaling. In contrast to the observation of a moderate genetic rescue of spermatogenesis in $Terc^{-/-}$ $p53^{-/-}$ mice and the striking rescue of the skin phenotype in $Acd^{acd/acd}$ $p53^{-/-}$ mice, we did not find any rescue of the testicular *acd* phenotype in $Acd^{acd/acd}$ $p53^{-/-}$ mice (Figure 2A) (Chin et al., 1999). Testes of $Acd^{acd/acd}$ mice of all *p53* genotypes either completely lacked (Figure 2B) or displayed severely reduced spermatogenesis (Figure 2A), with testis histology reminiscent of a Sertoli cell-only syndrome (SCOS). Total absence of germ cells in tubules without spermatogenesis was confirmed by Gcna immunohistochemistry (Figure 2A) (Enders and May, 1994). However, in some animals we observed areas of seminiferous tubules with normal spermatogenesis adjacent to empty seminiferous tubules, completely devoid of germ cells. Relative testicular weights were lower in $Acd^{acd/acd}$ animals regardless of their genetic *p53* status when compared to their $Acd^{+/+}$ littermates (Figure 2C). Due to the

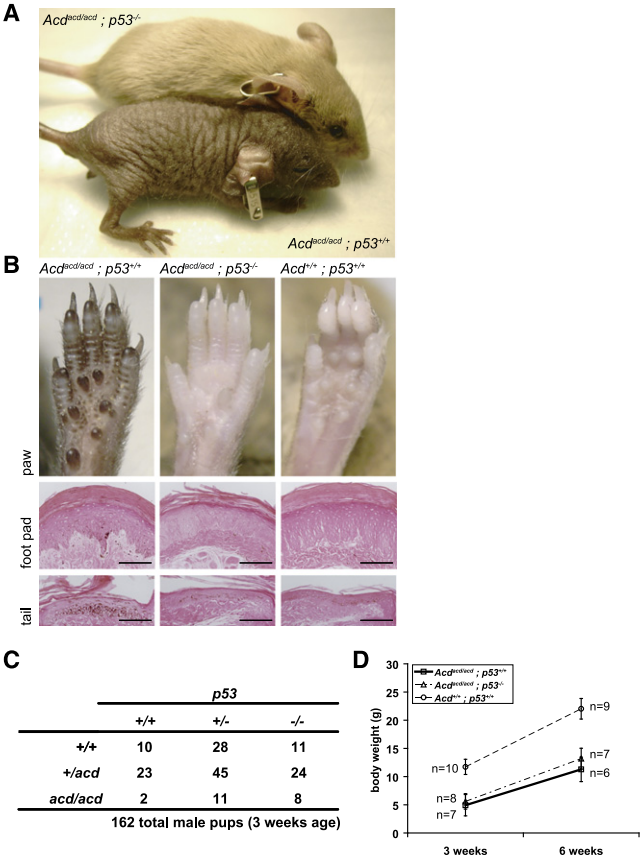

Figure 1. *p53* Ablation Reverses the Macroscopic Appearance of Adrenocortical Dysplasia Mice and Increases Perinatal Survival

(A) The macroscopic hyperpigmentation and fur phenotype of *Acd*$^{acd/acd}$ mice were completely rescued by *p53* ablation. Macroscopic appearance of 6-week-old mice: *Acd*$^{acd/acd}$ *p53*$^{-/-}$ mice shown on top of the picture showed normal fur growth and completely lacked hyperpigmentation. As a comparison, an *Acd*$^{acd/acd}$ *p53*$^{+/+}$ mouse is shown below.

(B) Hyperpigmentation is always present on the footpads of adrenocortical dysplasia mice. In *Acd*$^{acd/acd}$ *p53*$^{-/-}$ mice, the hyperpigmentation completely disappeared at the macroscopic level. Eosin-stained sections showed a striking reduction of pigment in the epidermis and dermis of *Acd*$^{acd/acd}$ *p53*$^{-/-}$ mice. The same results are shown for tail skin sections (scale bars for foot pads, 200 μm; for tails, 100 μm).

(C) Genotype analysis of 162 male pups at weaning age shows an increased survival for *Acd*$^{acd/acd}$ *p53*$^{-/-}$ mice. *Acd*$^{acd/acd}$ mice with either the *p53*$^{+/-}$ or the *p53*$^{+/+}$ genotype were not observed in the expected ratio ($p = 0.03$ and $p = 0.03$ vs. $p = 0.6$ for *p53*$^{-/-}$, χ^2 test).

(D) *Acd*$^{acd/acd}$ *p53*$^{-/-}$ mice are still smaller than their *Acd*$^{+/+}$ *p53*$^{+/+}$ littermates ($p < 10^{-7}$). Body weight did not differ from *Acd*$^{acd/acd}$ *p53*$^{+/+}$ mice ($p = 0.4$ at 3 weeks and $p = 0.1$ at 6 weeks, one-way ANOVA and F-test, data shown as mean ± SD). Postweaning weight gain was comparable in both *Acd*$^{acd/acd}$ groups to their *wt* littermates.

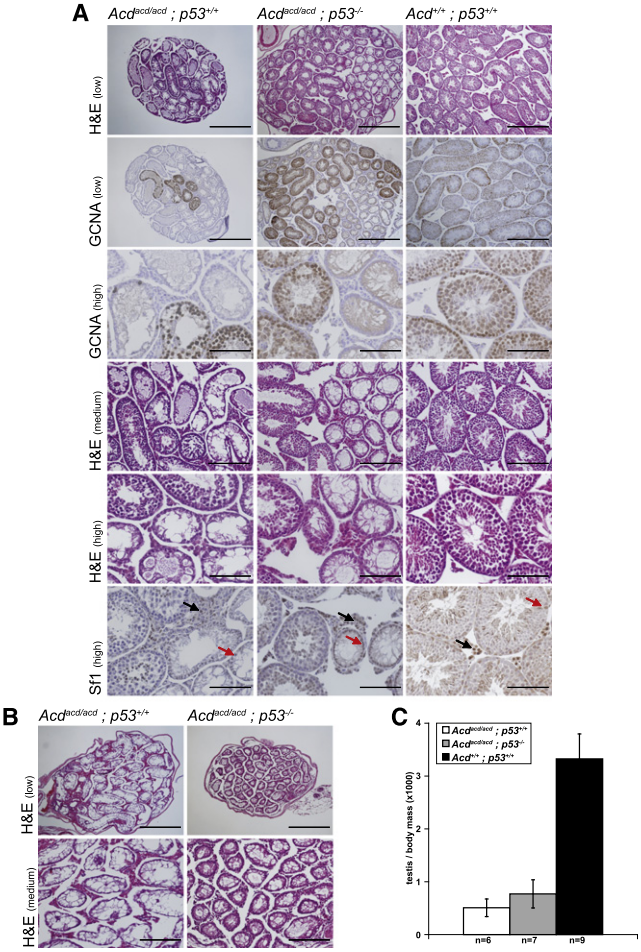

Figure 2. Loss of *p53* Does Not Rescue Spermatogenesis in *Acd*$^{acd/acd}$ Testes

Testes of *Acd*$^{acd/acd}$ mice display focal or complete absence of germinal epithelia reminiscent of Sertoli-cell-only syndrome regardless of their genetic *p53* status.

(A) Testes of *Acd*$^{acd/acd}$ *p53*$^{+/+}$ as well as *Acd*$^{acd/acd}$ *p53*$^{-/-}$ mice show focal spermatogenesis. Seminiferous tubules with an intact germinal cell epithelium harbored Gcna-positive germ cells. The Sf1-positive interstitial Leydig (black arrows) and Sertoli cell (red arrows) populations did not appear altered in either genotype compared to *Acd*$^{+/+}$ *p53*$^{+/+}$ littermates (scale bars for different levels of magnification: high, 100 μm; medium, 200 μm; and low, 400 μm).

(B) Some *Acd*$^{acd/acd}$ *p53*$^{+/+}$ and *Acd*$^{acd/acd}$ *p53*$^{-/-}$ testes completely lack spermatogenesis and germ cells. Only empty seminiferous tubules were present in these testes (scale bars for different levels of magnification: medium, 200 μm; and low, 400 μm).

(C) Testis weight relative to body weight is severely reduced in both *Acd*$^{acd/acd}$ *p53*$^{+/+}$ and *Acd*$^{acd/acd}$ *p53*$^{-/-}$ mice and therefore independent of their genetic *p53* status (*Acd*$^{+/+}$ *p53*$^{+/+}$ versus *Acd*$^{acd/acd}$ *p53*$^{-/-}$ $p = 1 \times 10^{-11}$, *Acd*$^{+/+}$ *p53*$^{+/+}$ versus *Acd*$^{acd/acd}$ *p53*$^{+/+}$ $p = 4 \times 10^{-12}$, *Acd*$^{acd/acd}$ *p53*$^{+/+}$ versus *Acd*$^{acd/acd}$ *p53*$^{-/-}$, $p = 0.19$, one-way ANOVA and F-test, data shown as mean ± SD).

infertility phenotype, male and female mice were regularly housed together and only on very rare occasions did we observe successful pregnancies. Because some components of the adult testis, specifically the Leydig cells, share a common developmental lineage and steroidogenic function with adrenocortical cells, we next examined morphology and characteristics of these interstitial testicular cells (Else and Hammer, 2005). The Leydig and Sertoli cell populations were morphologically normal, as evidenced by histologic analysis and Sf1 staining, a marker specific for these cell populations in the testis (Figure 2A) (Luo et al., 1995). The data indicate that, unlike the spermatogenic defect in *Terc*$^{-/-}$ mice, the germ cell failure of *Acd*$^{acd/acd}$ mice may not be caused by p53-mediated senescence or apoptosis and suggests that the *Acd*$^{acd/acd}$ decapping phenotype may

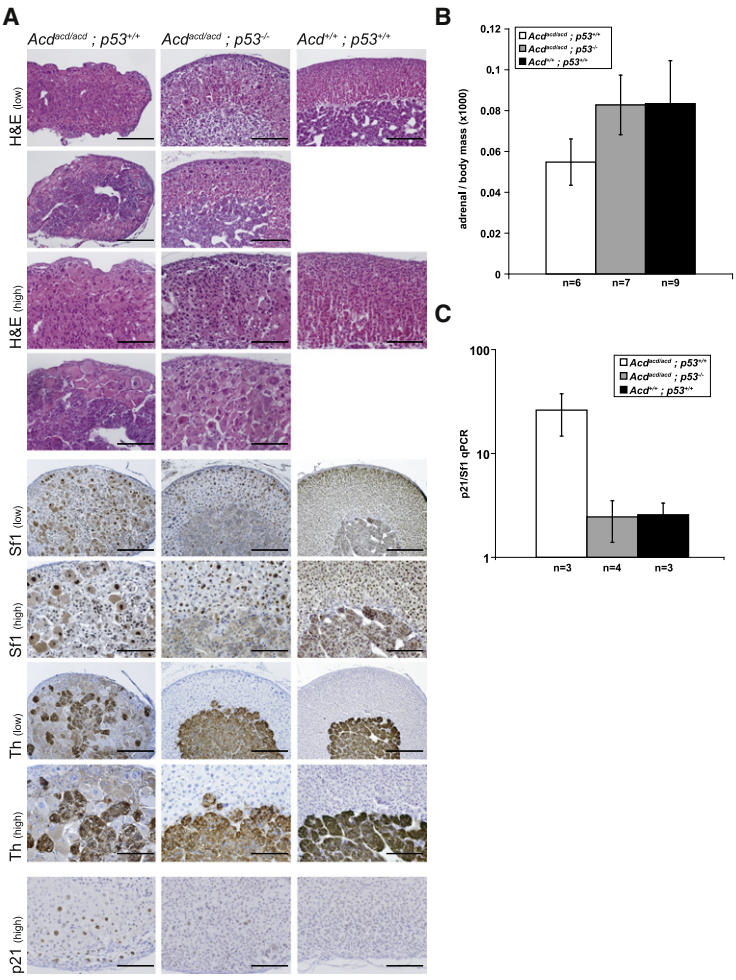

Figure 3. Adrenocortical Architecture, Weight, and *p21* Expression Is Normalized in Adrenal Cortex of *Acd*$^{acd/acd}$ *p53*$^{-/-}$ Mice

(A) The adrenal cortex of *Acd*$^{acd/acd}$ mice appears highly disorganized and consists of scattered cells with a high grade of nuclear pleomorphy. This phenotype was partially rescued in *Acd*$^{acd/acd}$ *p53*$^{-/-}$ mice, where adrenal glands appeared more clearly zonated and organized, while increased nuclear size and pleomorphy partially persisted. This became obvious using differentiation markers for the adrenal cortex (Sf1, steroidogenic factor 1) and for the adrenal medulla (Th, tyrosine hydroxylase). Two examples of adrenal glands from *Acd*$^{acd/acd}$ *p53*$^{+/+}$ and *Acd*$^{acd/acd}$ *p53*$^{-/-}$ and, as a comparison, one *wt* (*Acd*$^{+/+}$ *p53*$^{+/+}$) adrenal, are shown. *Acd*$^{acd/acd}$ *p53*$^{+/+}$ adrenal cortices stained positive for p21, a downstream mediator of p53-mediated senescence induction (scale bars for different levels of magnification: high, 100 μm; and low, 200 μm).

(B) Relative adrenal gland weight is normalized in *Acd*$^{acd/acd}$ *p53*$^{-/-}$ mice. Adrenal glands from *Acd*$^{acd/acd}$ *p53*$^{+/+}$ animals were about 66% the relative weight of *Acd*$^{+/+}$ *p53*$^{+/+}$ adrenal glands (*Acd*$^{acd/acd}$ *p53*$^{+/+}$ versus *Acd*$^{+/+}$ *p53*$^{+/+}$ p = 0.008, *Acd*$^{acd/acd}$ *p53*$^{+/+}$ versus *Acd*$^{acd/acd}$ *p53*$^{-/-}$ p = 0.005, *Acd*$^{acd/acd}$ *p53*$^{-/-}$ versus *Acd*$^{acd/acd}$ *p53*$^{+/+}$ p = 0.95, one-way ANOVA and F-test, data shown as mean ± SD).

(C) In *Acd*$^{acd/acd}$ *p53*$^{+/+}$ mice telomere deprotection induces *p21* expression as a marker of senescence. Ablation of *p53* strikingly reduced *p21* expression (*Acd*$^{acd/acd}$ *p53*$^{+/+}$ versus *Acd*$^{+/+}$ *p53*$^{+/+}$ p = 0.02, *Acd*$^{acd/acd}$ *p53*$^{+/+}$ versus *Acd*$^{acd/acd}$ *p53*$^{-/-}$ p = 0.03, *Acd*$^{acd/acd}$ *p53*$^{-/-}$ versus *Acd*$^{+/+}$ *p53*$^{+/+}$ p = 0.99, one-way ANOVA and F-test, data shown as mean ± SD).

not be identical to a short telomere phenotype or may be of a different degree of severity.

Absence of *p53* Partially Normalizes the Adrenocortical Phenotype

The main feature of the *acd* phenotype, which led to its name, is the characteristic dysmorphic small adrenal cortex (Beamer et al., 1994). In *acd* adrenal glands, there was variable intermingling of the normally distinct adrenal cortex and adrenal medulla, and a lack of the physiological concentric zonation of the mammalian adrenal cortex. Adrenocortical cells of *acd* animals displayed large eosinophilic cytoplasm and prominent enlarged pleomorphic nuclei sometimes harboring inclusion bodies. Remarkably, relative adrenal organ size was completely rescued in *Acd*$^{acd/acd}$ *p53*$^{-/-}$ mice, and an obvious albeit partial normalization of organ architecture with areas of a distinct cortical zonation was observed (Figures 3A and 3B). Moreover, although some areas of nuclear atypia remained, *Acd*$^{acd/acd}$ *p53*$^{-/-}$ adrenal cortices exhibited a partial rescue in cellular and nuclear size as well (Figure 3A).

Because telomere dysfunction in general and loss of *Tpp1/Acd* in particular are known to activate p53 signaling leading to cellular senescence, we examined whether p53-mediated cellular senescence contributed to the adrenal phenotype observed in *Acd*$^{acd/acd}$ mice. Although many adrenocortical cells in *Acd*$^{acd/acd}$ *p53*$^{+/+}$ mice stained positive for senescence-associated β-galactosidase, a reduced number of stained cells was observed in *Acd*$^{acd/acd}$ *p53*$^{-/-}$ adrenal cortices (Figure S3). Consistent with this observation was a reduction of *p21* gene expression (as determined by quantitative RT-PCR analysis) and a reduction in p21 protein (as determined by immunohistochemical analysis) in whole adrenal glands of *Acd*$^{acd/acd}$ *p53*$^{-/-}$ mice in comparison to *Acd*$^{acd/acd}$ *p53*$^{+/+}$ mice (Figures 3A and 3C). Caspase 3 and TUNEL staining was typically observed in *Acd*$^{+/+}$ *p53*$^{+/+}$ mice at the corticomedullary boundary only, where physiologic apoptosis normally occurs (data not shown). Specifically, there was no increase in cell number or intensity of cells that were positive for apoptotic markers in *Acd*$^{acd/acd}$ cortices. The changes in senescence-associated β-galactosidase activity and in *p21* expression levels, as well as the absence of positive markers of apoptosis, strongly argue for p53-dependent senescence induction as a main mechanism leading to the adrenocortical phenotype of *Acd*$^{acd/acd}$ *p53*$^{+/+}$ mice.

The *Acd*$^{acd/acd}$ Genotype Accelerates Tumorigenesis in *p53*$^{-/-}$ Mice

In *Terc*$^{-/-}$ mice, tumors can be observed at old age even without additional genetic challenge. Although we followed a relatively small cohort (5 animals) of *Acd*$^{acd/acd}$ *p53*$^{+/+}$ mice, we never observed tumors in either this specific aging cohort or in any other animal of this genotype in our colony (average mean [± SD] survival, 386 ± 78 days). The cause of death could not be determined in these mice, but the majority suffered from severe uni- or

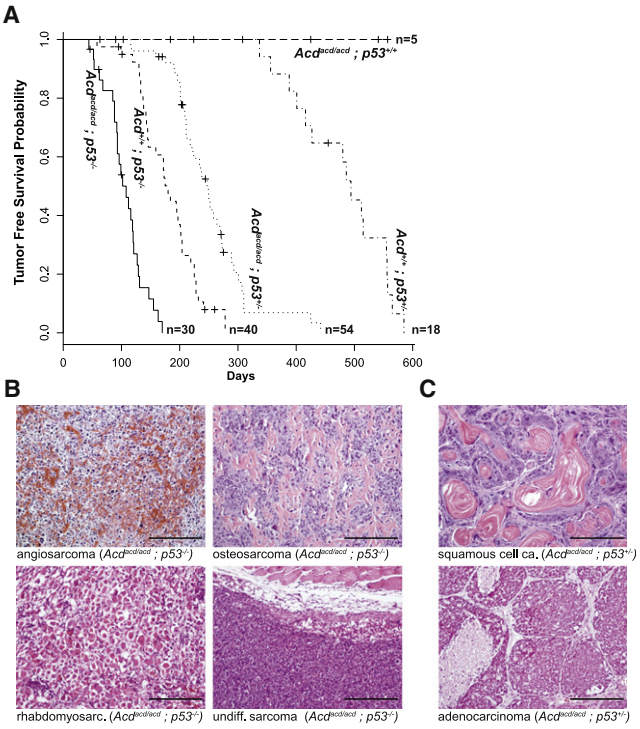

Figure 4. The *Acd*$^{acd/acd}$ Genotype Severely Reduces Tumor-Free Survival in *p53*$^{-/-}$ and *p53*$^{+/-}$ Mice

(A) Tumor-free survival is shown for the different genotype cohorts as a Kaplan-Meier plot. On average in both groups, *p53*$^{-/-}$ and *p53*$^{+/-}$, mice with the *Acd*$^{acd/acd}$ genotype developed tumors in approximately half the amount of time compared to their *Acd*$^{+/+}$ littermates (*Acd*$^{acd/acd}$ *p53*$^{-/-}$ *versus* *Acd*$^{+/+}$ *p53*$^{-/-}$ $p = 2 \times 10^{-11}$ and *Acd*$^{acd/acd}$ *versus* *p53*$^{+/-}$ *Acd*$^{+/+}$ *p53*$^{+/-}$ $p = 2 \times 10^{-9}$, log-rank test). In contrast, none of the *Acd*$^{acd/acd}$ *p53*$^{+/+}$ developed any tumors.

(B) The main categories of solid tumors in *Acd*$^{acd/acd}$ *p53*$^{-/-}$ and *Acd*$^{+/+}$ *p53*$^{-/-}$ are of the sarcoma spectrum (examples of angiosarcoma, osteosarcoma, rhabdomyosarcoma and undifferentiated sarcoma are shown; scale bars, 200 μm).

(C) In *Acd*$^{acd/acd}$ *p53*$^{+/-}$, but not *Acd*$^{+/+}$ *p53*$^{+/-}$, mainly carcinomas arose with a varying degree of squamous cell carcinoma or adenocarcinoma differentiation (scale bars, 200 μm).

bilateral hydronephrosis (Figure S2). Therefore, to investigate whether the accumulation of genomic alterations leads to increased tumorigenesis, a set of four animal groups with the *p53*$^{-/-}$ or *p53*$^{+/-}$ genotype and either *Acd*$^{acd/acd}$ or *Acd*$^{+/+}$ were analyzed for tumor development. Tumor-free survival of *Acd*$^{acd/acd}$ *p53*$^{-/-}$ mice was approximately half of that observed in *Acd*$^{+/+}$ *p53*$^{-/-}$ mice ($p = 2 \times 10^{-11}$) (Figure 4A). Macroscopic and histomorphological analysis of both genotypes identified a tumor spectrum comparable to previous studies of *p53*$^{-/-}$ and *Terc* $^{-/-}$ *p53*$^{-/-}$ mice. Most of the neoplastic lesions belonged to the lymphoma (46% in *Acd*$^{+/+}$ *p53*$^{-/-}$ mice and 38% in *Acd*$^{acd/acd}$ *p53*$^{-/-}$ mice) or sarcoma (44% in *Acd*$^{+/+}$ *p53*$^{-/-}$ mice and 47% in *Acd*$^{acd/acd}$ *p53*$^{-/-}$ mice) spectrum (Figure 4B; Table 1; Figure S4) (Donehower et al., 1992; Jacks et al., 1994). A subanalysis of tumor types of the sarcoma spectrum revealed angiosarcomas as the dominant tumor type in both groups, followed by undifferentiated sarcomas and rhabdomyosarcomas in *Acd*$^{acd/acd}$ *p53*$^{-/-}$ mice and fibrosarcomas in *Acd*$^{+/+}$ *p53*$^{-/-}$ mice. Interestingly, two tumors (6%) of the carcinoma spectrum were observed in the *Acd*$^{acd/acd}$ *p53*$^{-/-}$ but none were observed in the *Acd*$^{+/+}$ *p53*$^{-/-}$ group (Table 1).

Acd$^{acd/acd}$ *p53*$^{+/-}$ Mice Predominantly Develop Tumors of the Carcinoma Spectrum

As in the *p53*$^{-/-}$ groups, tumor risk was approximately doubled in *Acd*$^{acd/acd}$ *p53*$^{+/-}$ mice, compared with *Acd*$^{+/+}$ *p53*$^{+/-}$ mice ($p = 2 \times 10^{-9}$) (Figure 4A). Paralleling the reports for *Terc*$^{-/-}$ mice, we observed a remarkable difference in histological tumor types between these animal groups (Artandi et al., 2000). The main tumor type observed in *Acd*$^{+/+}$ *p53*$^{+/-}$ mice was sarcoma, with a preponderance of osteosarcomas. However, the majority of neoplasms in *Acd*$^{acd/acd}$ *p53*$^{+/-}$ animals were carcinomas, varying from squamous cell carcinomas (SCC) to adenocarcinomas, with a large fraction exhibiting adenosquamous differentiation (Figure 4C; Figure 5A; Table 1). The majority of these tumors identified by routine histological analyses also stained positive for pankeratin, confirming the diagnosis of carcinoma-type tumors (Figure 5A). Most carcinomas grew as subcutaneous lesions attached to the cutis and frequently presented with ulcerations, suggestive of an epidermal origin (Figure 5B). Although some of the SCCs appeared to directly arise from the epidermis, the adeno- and adenosquamous carcinomas may have their origin in epidermis-associated glands, such as sweat or mammary glands. Most interestingly, 5% of tumors were of adrenocortical origin as proven by positive Sf1 staining (Figure 5C; Figure 5D; Table 1). None of these adrenocortical cancers (ACC) stained positive for p21 (Figure 5C) as shown for the normal *acd* adrenal cortex (Figure 3A). This is further evidence that these tumor cells bypassed the senescent phenotype at some point in the process of neoplastic transformation. Finally, at least 11 of 16 tumors from *Acd*$^{acd/acd}$ *p53*$^{+/-}$ mice showed apparent loss of the *wt p53* allele, whereas at most 4 of 14 tumors from *Acd*$^{+/+}$ *p53*$^{+/-}$ mice showed a similar loss (Figure S5).

Genomic Alterations Underlying Tumorigenesis in *Acd*$^{acd/acd}$ Mice Are the Consequence of Dysfunctional Telomeres and Subsequent Breakage Fusion Bridge Cycles

Cells derived from *Acd*$^{acd/acd}$ animals display deprotected telomeres and acquire genomic aberrations (Else et al., 2007; Hockemeyer et al., 2007). Tumors from *Acd*$^{acd/acd}$ *p53*$^{-/-}$ mice showed a significant higher number of TIFs (Figures 6A and 6B). As further evidence that dysfunctional telomeres are the underlying mechanism of tumorigenesis, we observed a significantly higher percentage of anaphase bridges in tissue sections from tumors of *Acd*$^{acd/acd}$ animals (Figure 6C). Some of the mitotic figures with anaphase bridges revealed multiple strings of chromatin spanning the two poles of the dividing cells, and, in some cases, genomic material seemed to be localized or trapped between the two dividing poles, lacking a clear connection to either side (Figure 6D).

We next compared telomere length in neoplastic and nonneoplastic tissues from different genotypes. In contrast to previous cell culture experiments that reported an increase in telomere length, we did not observe a significant difference between nonneoplastic tissues from *Acd*$^{acd/acd}$ and *Acd*$^{+/+}$ animals (Figure 6E). Some degree of telomere shortening was observed

Table 1. Distribution of Tumor Types in the Different Genotypes

	acd/acd ; p53$^{-/-}$	*+/+ ; p53*$^{-/-}$	*acd/acd ; p53*$^{+/-}$	*+/+ ; p53*$^{+/-}$
Sarcoma	16 (47%)	18 (44%)	11 (26%)	9 (50%)
Angiosarcoma	7 (21%)	12 (29%)	0 (0%)	0 (0%)
Rhabdomyosarcoma	3 (9%)	1 (2%)	0 (0%)	0 (0%)
Osteosarcoma	2 (6%)	0 (0%)	4 (10%)	6 (33%)
MFH	1 (3%)	0 (0%)	2 (5%)	0 (0%)
Fibrosarcoma	0 (0%)	2 (5%)	0 (0%)	1 (6%)
Chondrosarcoma	0 (0%)	0 (0%)	1 (2%)	0 (0%)
Undifferentiated sarcoma	3 (9%)	3 (7%)	4 (10%)	2 (11%)
Carcinoma	2 (6%)	0 (0%)	27 (64%)	1 (6%)
Adenocarcinoma	1 (3%)	0 (0%)	8 (19%)	0 (0%)
Adenosquamous carcinoma	0 (0%)	0 (0%)	6 (14%)	0 (0%)
SCC	0 (0%)	0 (0%)	7 (17%)	1 (6%)
HCC	1 (3%)	0 (0%)	1 (2%)	0 (0%)
ACC	0 (0%)	0 (0%)	2 (5%)	0 (0%)
Undifferentiated carcinoma	0 (0%)	0 (0%)	3 (7%)	0 (0%)
Lymphoma	13 (38%)	19 (46%)	3 (7%)	7 (39%)
Germ cell	1 (3%)	1 (2%)	0 (0%)	1 (6%)
Brain	1 (3%)	2 (5%)	0 (0%)	0 (0%)
Undifferentiated/ not classified	1 (3%)	1 (2%)	1 (2%)	0 (0%)
Total	34 (100%)	41 (100%)	42 (100%)	18 (100%)

Animals were autopsied at the time of either spontaneous death or visible tumor growth. Tumors from *Acd*$^{acd/acd}$ *p53*$^{+/-}$ mice had an overall higher occurrence of tumors of the carcinoma spectrum ($p = 1 \times 10^{-14}$, two-sided Fisher's Exact test). Carcinomas and sarcomas are broken down in distinct tumor diagnosis. Most of the *Acd*$^{acd/acd}$ *p53*$^{+/-}$ tumors were of a squamous cell carcinoma, adenocarcinoma, or adenosquamous carcinoma differentiation type. All other tumor types fell into the typical spectrum of *p53*$^{-/-}$ tumors (i.e., sarcomas and lymphomas).

in some tumors, compared with nonneoplastic tissue, regardless of whether they were from *Acd*$^{acd/acd}$ or *Acd*$^{+/+}$ animals. This is in contrast to the *Terc*$^{-/-}$ mouse model, where progressive telomere shortening provides the basis for telomere dysfunction. Anaphase bridges are viewed as one morphological correlate of breakage-fusion bridge cycles (BFBs). Therefore, we analyzed tumors and a tumor cell line by comparative genomic hybridization (CGH) and spectral karyotyping, respectively. In CGH analysis, multiple amplifications as well as areas of "step-like" amplifications were present in the genome from *Acd*$^{acd/acd}$ tumors (Figures 7A and 7B; Figure S6). These alterations are an expected result of recurrent BFBs. The average number of segments deviating from the normal tissue baseline was higher in *Acd*$^{acd/acd}$ than *Acd*$^{+/+}$ tumors (90.6 ± 38.4 transition points versus 27 ± 8.3 transition points, $p = 0.0048$) (Figure 7A). As this analysis may be influenced by simple background noise of the hybridization analysis, we next identified the number of chromosomes affected by copy number alterations. There were significantly more chromosomes with at least one copy number change in *Acd*$^{acd/acd}$ than *Acd*$^{+/+}$ tumors. Notably, several of the observed amplifications encompass loci that may contribute to tumorigenesis. This includes amplifications of potential or proven oncogenes, such as the cluster of *Wnt* genes on chromosome 11 and the *Kras* locus on chromosome 6, which has recently been shown to be amplified in tumors from *Terc*$^{-/-}$ mice. As a proof of principle, we found very specific rearrangements by spectral karyotyping analysis of an *Acd*$^{acd/acd}$ *p53*$^{-/-}$ rhabdomyosarcoma cell line, consisting of segments of two different chromosomes in an alternating pattern (Figure 7C). These alterations are likely due to reoccurring BFBs involving two different chromosomes and represent the cytogenetic correlate of the stepwise regional amplifications found in CGH analysis.

DISCUSSION

In this study, we show that the ablation of *p53* both profoundly rescues a number of characteristics of the *acd* phenotype and increases tumorigenesis. These results underscore the importance of p53 activation as a driving force in the development of major characteristics of the adrenocortical dysplasia phenotype. The *acd* mouse is the first viable animal model that permits analysis of the selective deficiency of an integral part of the shelterin complex. Moreover, *acd* mice allow for analysis of the contribution of telomere deprotection in the absence of telomere shortening to genetic instability and tumorigenesis. In contrast, telomere dysfunction in *Terc*$^{-/-}$ mice is less defined and is observed only after significant telomere shortening following breeding over successive generations. Deprotection versus shortening may underlie the distinct phenotypes of *acd* mice and *Terc*$^{-/-}$ mice.

Phenotypic rescue through the ablation of *p53* in the *Acd*$^{acd/acd}$ mice was most profound in the skin, where hyperpigmention was macroscopically completely absent in *Acd*$^{acd/acd}$ *p53*$^{-/-}$ mice. Two possible scenarios are discussed as the basis for hyperpigmentation in *acd* mice. Elevated ACTH and MSH levels in the

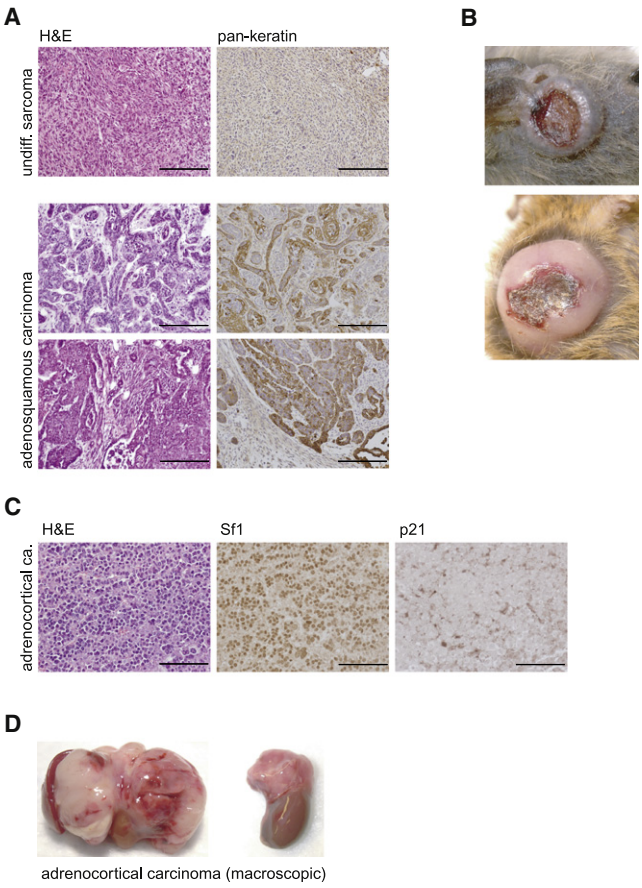

Figure 5. $Acd^{acd/acd}$ $p53^{+/-}$ Mice Predominantly Develop Carcinomas

(A) Some $Acd^{acd/acd}$ $p53^{+/-}$ carcinomas show an intermediate adenosquamous differentiation type with elements of squamous cell as well adenocarcinoma-like elements. Skin associated carcinomas stained highly positive for pankeratin (scale bars, 200 μm).

(B) Most carcinomas arise in the cutaneous or subcutaneous regions and typically show central necrosis.

(C) Five percent of $Acd^{acd/acd}$ $p53^{+/-}$ develop adrenocortical cancers. Their origin could readily be identified by positive Sf1 staining. Adrenocortical cancers were p21 negative, indicating that they evaded senescence (scale bars, 100 μm).

(D) Macroscopically, adrenocortical cancer expanded within the peritoneal cavity adhering to adjacent organs. Two examples of ACC from $Acd^{acd/acd}$ $p53^{+/-}$ mice are shown.

setting of adrenocortical insufficiency could directly stimulate melanocytes, or, alternatively, melanocytes that progressed to senescence could be more active in terms of pigment production. The first possibility seems to be unlikely because mouse models of adrenocortical insufficiency, such as the $Mc2r^{-/-}$ (ACTH receptor) mouse, do not develop hyperpigmentation (personal communication D. Chida) (Chida et al., 2007). Furthermore, we were not able to detect significant differences in baseline ACTH and corticosterone levels (data not shown). Overall it seems more likely that skin hyperpigmentation is induced by telomere deprotection and direct activation of p53-sensitive pathways in melanocytes as it has been shown for other mouse models (Atoyan et al., 2007; Cui et al., 2007; Hadshiew et al., 2008; Khlgatian et al., 2002).

Male germ cells have a very high proliferative rate and, therefore, seem to depend more than other tissues on telomere integrity and perhaps telomerase activity (Hemann et al., 2001; Lee et al., 1998). We did not observe any rescue of the testicular $Acd^{acd/acd}$ phenotype through *p53* ablation in $Acd^{acd/acd}$ animals, which is in contrast to the moderate rescue observed in late generation $Terc^{-/-}$ $p53^{-/-}$ mice (Chin et al., 1999). Therefore, it can be hypothesized that, unlike other tissues, germ cells do not completely depend on p53-sensitive pathways to induce their removal from the proliferative cell pool. It is also possible that different degrees of severity of telomere dysfunction can induce alternative pathways in an organ-dependent manner. The observation of completely empty SCOS-like tubules adjacent to seminiferous tubules with grossly normal spermatogenesis suggests a developmental defect in $Acd^{acd/acd}$ mice, as it seems unlikely that the complete germ cell epithelium of some tubules but not others disappears at the same time as the result of postnatal germ cell failure. For a degenerative mechanism in adult life, one would expect random losses of germ cells and an overall reduction of spermatogenesis rather than the observed "all-or-nothing" phenomenon. It is worth mentioning that *TPP1/ACD* expression and telomerase activity are reduced in biopsies of SCOS testes (Feig et al., 2007; Schrader et al., 2002).

A main characteristic of the *acd* phenotype is cytomegalic adrenal hypolplasia congenita (AHC), which is not observed in late generation $Terc^{-/-}$ mice (data not shown) and has not been reported for any other mouse model of telomere dysfunction. In this study, we show that the adrenal *acd* phenotype is caused by the induction of p53-dependent senescence. In the adrenal cortex of $Acd^{acd/acd}$ $p53^{-/-}$ mice, we observe a normalization of organ size and architecture. In humans, cytomegalic AHC is observed in random pediatric or fetal autopsies as well as part of several syndromes. The majority of humans with cytomegalic AHC (with hypogonadotropic hypogonadism) have a germ line mutation in *NR0B1* (*DAX1*) (Achermann et al., 1999; Zanaria et al., 1994). The emerging role of NR0B1 in embryonic and tumor stem cell physiology suggests that cytomegalic adrenal failure may reflect a common morphological end point of stem cell failure and exhaustion of organ maintenance capacity due to a number of causes, including telomere dysfunction (Kim et al., 2008; Mendiola et al., 2006; Niakan et al., 2006).

In summary, ablation of *p53* rescues the $Acd^{acd/acd}$ phenotype to varying degrees and in an organ-specific manner. The differences of the $Acd^{acd/acd}$ and the $Terc^{-/-}$ phenotype and their different rescue by *p53* ablation can be explained by distinct molecular mechanisms induced by either short telomeres or deprotected telomeres. Alternatively, telomere dysfunction induced by deprotection in $Acd^{acd/acd}$ mice could be more severe than telomere dysfunction induced by telomere shortening in $Terc^{-/-}$ mice and therefore not as readily rescued by simple *p53* ablation. Indeed, one would expect some telomere deprotection on every telomere in $Acd^{acd/acd}$ mice due to the severe deficiency in Tpp1/Acd as opposed to $Terc^{-/-}$ mice, where telomere decapping gradually develops with the loss of telomere sequences, resulting in the inability to bind shelterin components. Furthermore, it would be of interest to investigate potential roles of TPP1/Acd independent of its function in telomere protection. Such functions have been discovered for the

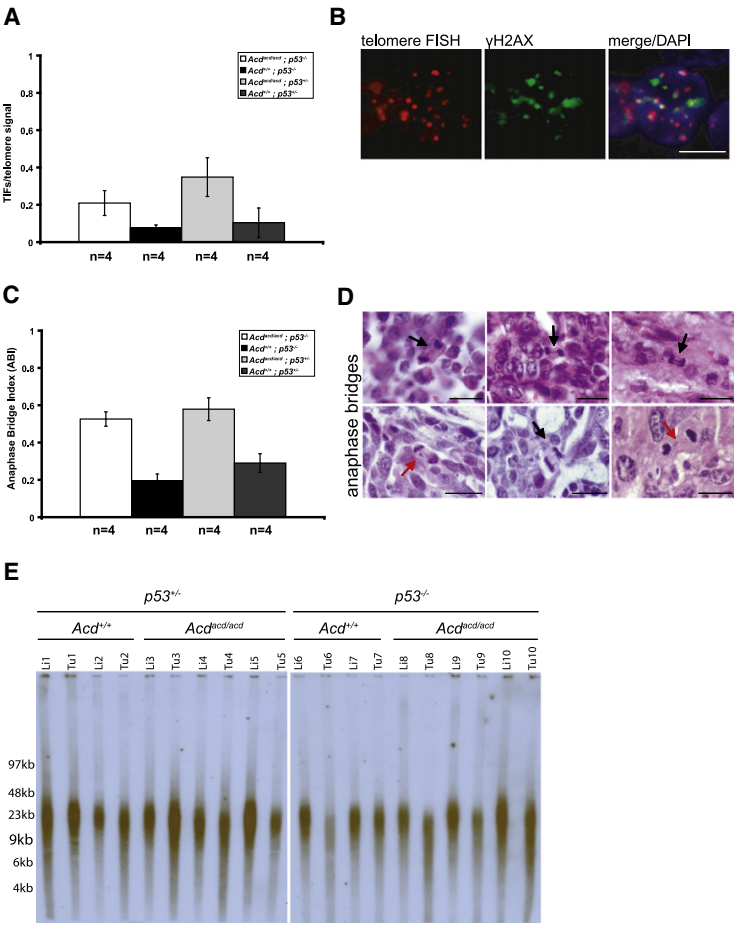

Figure 6. Tumors from *Acd*$^{acd/acd}$ Mice Exhibit Hallmarks of Genomic Instability in the Absence of Significant Telomere Shortening

(A) *Acd*$^{acd/acd}$ tumors had significantly more telomere dysfunction-induced foci (TIFs) per total telomere signals than did *Acd*$^{+/+}$ tumors, indicating that telomere decapping is evident in these neoplasms ($p = 0.047$ for *Acd*$^{acd/acd}$ *p53*$^{-/-}$ versus *Acd*$^{+/+}$ *p53*$^{-/-}$ tumors and $p = 0.002$ for *Acd*$^{acd/acd}$ *p53*$^{+/-}$ versus *Acd*$^{+/+}$ *p53*$^{+/-}$ tumors, one-way ANOVA and F-test, data shown as mean ± SD).

(B) Decapped telomeres recruit factors of the DNA surveillance machinery, such as γH2ax, and form TIFs. TIFs, the classical co-localization of telomere FISH signal (red), and γH2ax immunohistochemistry (green) were observed in *Acd*$^{acd/acd}$ tumors (scale bars, 5 μm).

(C) Tumors from *Acd*$^{acd/acd}$ mice (*p53*$^{-/-}$ or *p53*$^{+/-}$) have a significantly increased anaphase bridge index (*Acd*$^{acd/acd}$ *p53*$^{-/-}$ versus *Acd*$^{+/+}$ *p53*$^{-/-}$ $p = 5 \times 10^{-5}$ and *Acd*$^{acd/acd}$ *versus p53*$^{+/-}$ *Acd*$^{+/+}$ *p53*$^{+/-}$ $p = 0.001$, one-way ANOVA and F-test, data shown as mean ± SD).

(D) Classical anaphase bridges, a morphological correlate of breakage-fusion-bridge cycles (BFBs), are present in tumors from *Acd*$^{acd/acd}$ mice (black arrows). In some instances, chromosomal material (red arrows) appeared in between the two poles without a clear connection to either of the poles of the emerging daughter cells (scale bars, 20 μm).

(E) Telomere length as measured by TRF gel analysis. No clear differences between normal tissues (liver) of different genotypes were observed. The *Acd*$^{acd/acd}$ genotype itself did not lead to in vivo telomere length alteration in normal tissues. Some *Acd*$^{acd/acd}$ as well as *Acd*$^{+/+}$ tumors showed a moderate shortening of telomere length.

protein component of telomerase TERT that participates in telomere-independent stem cell physiology (Choi et al., 2008; Sarin et al., 2005).

The onset of tumor development was significantly accelerated in *Acd*$^{acd/acd}$ *p53*$^{-/-}$ and *Acd*$^{acd/acd}$ *p53*$^{+/-}$ mice, compared with their *Acd*$^{+/+}$ *p53*$^{-/-}$ *and Acd*$^{+/+}$ *p53*$^{+/-}$ littermates, respectively. This underscores the role of telomere dysfunction in the induction of tumorigenesis as it has been described for *Terc*$^{-/-}$ mice (Artandi et al., 2000; Chin et al., 1999). For the *Acd*$^{acd/acd}$ phenotype, the sole driving force for genomic instability can be attributed to the telomere deprotection phenotype (Else et al., 2007; Hockemeyer et al., 2007). In contrast to the *Terc*$^{-/-}$ mice, no telomere shortening was necessary for tumor development. Though our experiments do not entirely exclude the possibility that a small fraction of telomeres reach a critical short length and dysfunctional state, this possibility seems to be unlikely because we did not observe any differences in telomere length comparing normal tissues from *Acd*$^{acd/acd}$ and *Acd*$^{+/+}$ animals. Some degree of telomere shortening was inconsistently observed comparing tumor tissue and normal tissue (liver) from the same animal and was independent of the *Acd* genotype. Furthermore, a hallmark of telomere dysfunction in *Terc*$^{-/-}$ mice is the presence of chromosomal fusions lacking telomere signals at the fusion site (Hande et al., 1999). In contrast, we have previously shown that telomere signals are detectable at the nonhomologous fusion sites in *Acd*$^{acd/acd}$ MEFs (Else et al., 2007). The lack of significant telomere length differences between *Acd*$^{acd/acd}$ and *Acd*$^{+/+}$ animals shows that *Tpp1/Acd* deficiency in vivo does not lead to average telomere length differences, as opposed to reports in human cells where the acute loss of *TPP1/ACD*, or the use of a dominant negative isoform, leads to excessive telomere lengthening (O'Connor et al., 2006; Xin et al., 2007; Ye et al., 2004).

Considering the role of telomeres and telomerase in the telomere-based two-step model of carcinogenesis, the *acd* mouse is a useful tool to selectively investigate the in vivo consequences of telomere deprotection (Artandi and DePinho, 2000; Cosme-Blanco et al., 2007; Ju and Rudolph, 2006). Telomere dysfunction is hypothesized to lead to genomic shuffling via BFBs, which contributes to tumorigenesis. Later, the genome becomes stabilized through a telomere maintenance mechanism such as telomerase activity or alternative telomere length maintenance mechanisms (ALT) (Farazi et al., 2003; Maser and DePinho, 2002; Rudolph et al., 2001). Telomere deprotection has been recently suggested to participate in oncogenesis in a variety of human cancers (Poncet et al., 2008; Vega et al., 2008). Our studies of the *Acd*$^{acd/acd}$ *p53*$^{-/-}$ mouse model reproduce the genomic alterations proposed by the telomere-based model of carcinogenesis (Chin et al., 2004; O'Hagan et al., 2002). The multiple chromosomal amplifications and cytogenic changes observed in *Acd*$^{acd/acd}$ tumors together with an increased number of anaphase bridges support BFBs as a main mechanism of ongoing genomic alterations in tumorigenesis. Additionally, we argue that BFB-induced losses of genetic material are

A

Acd genotype	*p53* genotype	transitions	selected segments	runs	chromosomes	chromosomes with amplicons (deletions)
acd/acd	+/-	80	1	1	1	X
acd/acd	+/-	143	66	36	10	1,3,4,5,6,10,11,13,16, (19)
acd/acd	+/-	66	6	6	4	1,3,11, (10)
acd/acd	-/-	134	1	1	1	X
acd/acd	-/-	71	2	2	2	(6,14)
acd/acd	-/-	50	25	10	3	5,6,X
+/+	+/-	16	0	0	0	
+/+	+/-	34	7	6	2	(8,14)
+/+	-/-	33	9	1	1	9
+/+	-/-	25	0	0	0	
1-sided, (Wilcoxon) Rank-sum test		0.0048	0.23	0.064	0.041	

B

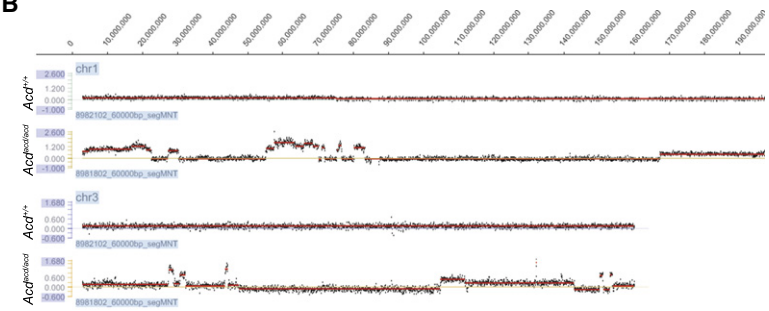

C

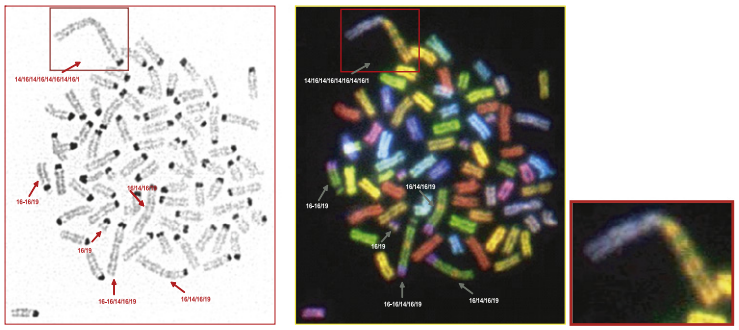

Figure 7. Telomere Deprotection in Tumors from *Acd*$^{acd/acd}$ Mice Leads to Genomic and Cytogenetic Alterations as a Consequence of Breakage Fusion Bridge Cycles

(A) Table summarizing characteristics of *Acd*$^{acd/acd}$ tumors as analyzed by CGH. *Acd*$^{acd/acd}$ tumors have significantly more transition points, compared with *Acd*$^{+/+}$ tumors, as would be expected with repeated BFBs, and significantly more chromosomes exhibited copy number alterations.

(B) CGH example of tumor DNA normalized to same animal liver DNA. Multiple amplifications sometimes presenting in a stepwise manner of increasing amplification values on the same chromosome (e.g., chr. 1 and chr. 3 of two samples) were observed in *Acd*$^{acd/acd}$ (lower panel) but not in *Acd*$^{+/+}$ tumors (upper panel) (y axis: $\log_2$ of tumor/liver).

(C) Spectral karyotyping of a cell line derived from a *Acd*$^{acd/acd}$ *p53*$^{-/-}$ rhabdomyosarcoma revealed genomic rearrangements in the form of hybrid chromosomes consisting of genomic stretches of original chromosome 16 and chromosome 19 (see magnification lower right).

also responsible for the increased frequency of loss of the *wt p53* allele in *Acd*$^{acd/acd}$ *p53*$^{+/-}$ versus *Acd*$^{+/+}$ *p53*$^{+/-}$ tumors.

The observations of marked senescence in the adrenal cortex of *Acd*$^{acd/acd}$ mice and the development of ACC in *Acd*$^{acd/acd}$ *p53*$^{+/-}$ mice suggest that the escape from senescence may contribute to adrenocortical carcinogenesis. Although ACC is not the main neoplasia (5% of tumors in *Acd*$^{acd/acd}$ *p53*$^{+/-}$ mice) observed in this study, it is a finding of great importance as there is currently no mouse model that specifically develops ACC. ACC in humans is a rare disease with a dismal prognosis. Mouse models of telomere dysfunction may be further exploited to study this rare type of cancer and may serve as a useful tool to understand the pathogenesis and pathophysiology of this disease. In humans, ACC is one of the syndrome-defining pathologies in Li-Fraumeni syndrome. The specific occurrence of this tumor in *Acd*$^{acd/acd}$ *p53*$^{+/-}$ mice may further suggest a participation of telomere dysfunction in Li-Fraumeni-associated carcinogenesis. Indeed it has recently been shown that telomere length correlates with age at tumor onset in patients with Li-Fraumeni syndrome (Tabori et al., 2007).

It has been assumed for a long time that telomere deprotection can provide the basis for generating a procancer genome during tumorigenesis in human tissues. We believe that the *acd* mouse provides an excellent model for the in vivo dissection of these mechanisms underlying this phenomenon and will increase our understanding of how telomere pathophysiology impacts the origin of tumors in mammalian organisms. Lastly *TPP1/ACD* and other genes of the shelterin complex may facilitate both our understanding of a genetic basis in patients with dyskeratosis congenita-like heritable cancer syndromes that do not exhibit significant changes in overall telomere length.

EXPERIMENTAL PROCEDURES

Animal Procedures

All experiments involving animals were performed in accordance with institutionally approved and current animal care guidelines (UCUCA-09458). Adrenocortical dysplasia (*acd*) mice used in this study were from a mixed DW/JxCAST/Ei background and were genotyped as described elsewhere (Keegan et al., 2005). *p53*$^{-/-}$ mice (C57BL6/J; *Trp53*^{tm1Tyj}) were purchased from Jackson Laboratories (JAX mice and Services, Bar Harbor, ME) and were genotyped as described elsewhere (Jacks et al., 1994). Double heterozygous animals (*Acd*$^{+/acd}$ *p53*$^{+/-}$) were crossed to generate the genotypes used in this study. A series of animals ($\geq$5) of each genotype were weighed at 3 weeks and 6 weeks. Initially, autopsies were conducted at 6 weeks of age, when organ weights of adrenal glands and testis were recorded and tissues were either preserved for histological analysis or snap frozen for RNA preparation. For survival studies, autopsy was conducted either at the time of obvious tumor growth or at spontaneous death. Some tumor samples were used to establish cell lines. Parts of the tumor were disintegrated using cell strainers, washed in PBS and grown on fibronectin-coated plates (Sigma, St. Louis, MO) in DMEM supplemented with 5% FBS and antifungal, antibacterial solution (all Invitrogen, Carlsbad, CA). The χ^2 test was used to test the amount of observed pups with the *Acd*$^{acd/acd}$ genotype within a certain *p53* genotype. Survival between groups was analyzed with log-rank tests. Animals without obvious tumor, or in which degradation precluded meaningful analysis or with a histological benign pathology, were considered censored at the time of death.

Histology and Immunohistochemistry

For general histological analysis, tissues were fixed in 4% formaldehyde, dehydrated, and paraffin embedded; 6-μm sections were used for routine hematoxylin and eosin staining or further immunohistological procedures.

Immunohistochemical analyses followed standard protocols using the ABC Elite kit (Vector Laboratories, Burlingame, CA) and DAB Sigma Fast (Sigma, St. Louis, MO) or fluorescent secondary antibodies. Primary antibody incubation was done at 4°C overnight. Primary and secondary antibodies were used at the following concentrations: p21 (1:50, mouse monoclonal, #556430, BD Biosciences, San Jose, CA), GCNA (1:200, rat monoclonal IgM, obtained from G.C. Enders [Enders and May, 1994]), Sf1 (1:1000, provided by Kenichirou Morohashi), pan-keratin (1:100, mouse monoclonal, #MS343, Lab Vision, Fremont, CA), γH2ax (1:50, #2577 Cell Signaling, Danvers, MA), biotinylated anti-mouse (1:200, BA9200, Vector Laboratories, Burlingame, CA), biotinylated anti-rabbit (1:200, BA1000, Vector Laboratories, Burlingame, CA), biotinylated-anti-rat (1:200, #161603, KPL, Gaithersburg, MD), and Alexa-Fluor 486-coupled anti-mouse IgG (1:200, #A11029, Carlsbad, CA). Telomere FISH procedure was conducted as described previously following a protocol modified from Meeker et al. (2002) (Else et al., 2008). Pictures were taken and in plane telomere signals were counted (at least 250/slide) in nuclei with positive γH2ax staining. The ratio of telomeres with to telomeres without colocalizing γH2ax staining (TIFs) was calculated for at least 4 tumors per group. Anaphase bridges and anaphase mitoses were counted in ≥4 tumors per genotype. The anaphase bridge index was calculated as the ratio of anaphase bridges per total metaphases. Pathological diagnosis was made in synopsis of macroscopic and microscopic pathologies. Images were captured with an Optiphot-2 microscope (Nikon, Melville, NY) with a DP-70 camera and software system (Olympus, Hauppauge, NY). For comparative immunohistochemical analyses, system and software processing (Adobe Photoshop, Adobe Illustrator, San Jose, CA) settings were kept constant over sample groups. For statistical analysis, data were fit using a one-way ANOVA, and pairs of groups were compared using the resulting F-tests.

Reverse Transcribed Quantitative Polymerase Chain Reaction

RNA was extracted from adrenal glands by a standard method using TRIzol (Invitrogen, Carlsbad, CA). RNA was quantified and reverse transcription was performed using the i-Script kit (Bio-Rad, Hercules, CA) following the manufacturer's protocol. Intron-spanning primers were used for Gapdh (forward, 5′-TGT CCG TCG TGG ATC TGA C-3′; reverse, 5′-CCT GCT TCA CCA CCT TCT TG-3′), Sf1 (forward, 5′-ACA AGC ATT ACA CGT GCA CC-3′; reverse, 5′-TGA CTA GCA ACC ACC TTG CC-3′), and p21 (Cdkn1a) (forward 5′-TCC ACA GCG ATA TCC AGA CA-3′; reverse, 5′-GGA CAT CAC CAG GAT TGG AC-3′) (Invitrogen, Carlsbad, CA). For the PCR, double concentration SYBR Green PCR master mix was used in an ABI 7300 thermocycler (both Applied Biosystems, Foster City, CA). For statistical analysis, data were fit using a one-way ANOVA, and pairs of groups were compared using F-tests.

Telomere Restriction Fragment Length Assay

Telomere restriction fragment (TRF) analysis utilized published protocols with modifications (Else et al., 2008; Hemann and Greider, 2000). A purification kit (#13343, QIAGEN, Hilden, Germany) was used to obtain high molecular weight genomic DNA; 2 μg of genomic DNA was digested with 60 U of Dpn II for 36 hr and run in 1% agarose (Seakem, Lonza, Rockland, ME) using a CHEF mapper (BioRad, Hercules, CA). The automatic algorithm was set to a range of 5 kb to 200 kb. A PFG low molecular weight marker (NEB, Ipswich, MA) was used as a size marker. DNA-gels were further processed as described elsewhere (Else et al., 2008).

Comparative Genomic Hybridization

Isolated high molecular weight genomic DNA (#13343, QIAGEN, Hilden, Germany) from 6 *acd* tumors and 4 *wt* tumors was run on a 1% agarose gel, and spectrophotometric measurements at 230 nm, 260 nm and 280 nm were conducted to exclude samples with significant degradation or contamination. Comparative genomic hybridization (CGH) was conducted on the CGH0150-WMG platform using the NimbleGen service (NimbleGen, Madison, WI). The raw data are available in ArrayExpress (experiment E-TABM-680). The NimbleGen CGH-SegMNT algorithm was used to divide chromosomes into segments that were separated by transitions in the logarithm of test to reference sample ratios. We excluded data from the Y chromosome (which had a lower probe density) as well as small segments represented by 30 or fewer probes. The software created segments even when the change in average estimated log-ratio was very small. Consequently, we selected segments as abnormal if the base-2 log-ratio was greater than 0.5 or less than −0.5, or if the log-ratio was larger than 0.3 in absolute value and the change in log-ratio from the previous segment was also greater than 0.3. The second criterion selects segments where the change in copy number was abrupt, whereas the first criterion selects a segment even if the estimated log-ratio rises and falls gradually. We combined neighboring selected segments that were all estimated to have copy numbers greater than 2, or all less than 2, into "runs," and counted the number of distinct runs in each tumor. We counted the total number of chromosomes containing selected segments for each tumor, and compared these and the other metrics between $Acd^{acd/acd}$ and $Acd^{+/+}$ tumors using one-sided Rank-Sum tests.

Karyotypic Analyses

Metaphases were generated using standard procedures. Slides were then subjected to SKY analysis using mouse SKY paint mixture from Applied Spectral Imaging (ASI, Vista, CA) according to the manufacturer's protocol. All imaging was performed on an Olympus BX-61 microscope equipped with an interferometer driven by a desktop computer and specialized software (ASI, Vista, CA). Inverted DAPI images were generated using SKYview software (ASI, Vista, CA).

ACCESSION NUMBERS

CGH data have been deposited in ArrayExpress, experiment E-TABM-680.

SUPPLEMENTAL DATA

Supplemental Data include Supplemental Experimental Procedures and six figures and can be found with this article online at http://www.cell.com/cancer-cell/supplemental/S1535-6108(09)00145-7.

ACKNOWLEDGMENTS

T.E. and A.T. were sponsored through generous scholarships by the Garry Betty Foundation. This work has been sponsored by grant NIH NIDDK DK62027 (G.D.H.) and a grant from the Sidney Kimmel Cancer Research Foundation (D.O.F.). The authors would like to thank the DNA sequencing core facility at the University of Michigan, Tom Giordano for his endocrine pathology expertise, Buffy Ellsworth from Sally Camper's laboratory for IHC advice, and Jose Luis Garcia Perez for intellectual exchange and experimental advice, as well as Guido Bommer, Joanne Heaton, Catherine Keegan, and Sonalee Shah for editorial advice.

Received: November 2, 2008
Revised: March 1, 2009
Accepted: April 27, 2009
Published: June 1, 2009

REFERENCES

Achermann, J.C., Gu, W.X., Kotlar, T.J., Meeks, J.J., Sabacan, L.P., Seminara, S.B., Habiby, R.L., Hindmarsh, P.C., Bick, D.P., Sherins, R.J., et al. (1999). Mutational analysis of DAX1 in patients with hypogonadotropic hypogonadism or pubertal delay. J. Clin. Endocrinol. Metab. *84*, 4497–4500.

Artandi, S.E. (2002). Telomere shortening and cell fates in mouse models of neoplasia. Trends Mol. Med. *8*, 44–47.

Artandi, S.E., and DePinho, R.A. (2000). A critical role for telomeres in suppressing and facilitating carcinogenesis. Curr. Opin. Genet. Dev. *10*, 39–46.

Artandi, S.E., Chang, S., Lee, S.L., Alson, S., Gottlieb, G.J., Chin, L., and DePinho, R.A. (2000). Telomere dysfunction promotes non-reciprocal translocations and epithelial cancers in mice. Nature *406*, 641–645.

Atoyan, R.Y., Sharov, A.A., Eller, M.S., Sargsyan, A., Botchkarev, V.A., and Gilchrest, B.A. (2007). Oligonucleotide treatment increases eumelanogenesis, hair pigmentation and melanocortin-1 receptor expression in the hair follicle. Exp. Dermatol. *16*, 671–677.

Beamer, W.G., Sweet, H.O., Bronson, R.T., Shire, J.G., Orth, D.N., and Davisson, M.T. (1994). Adrenocortical dysplasia: a mouse model system for adrenocortical insufficiency. J. Endocrinol. *141*, 33–43.

Blasco, M.A. (2005). Telomeres and human disease: ageing, cancer and beyond. Nat. Rev. Genet. *6*, 611–622.

Blasco, M.A., Lee, H.W., Hande, M.P., Samper, E., Lansdorp, P.M., DePinho, R.A., and Greider, C.W. (1997). Telomere shortening and tumor formation by mouse cells lacking telomerase RNA. Cell *91*, 25–34.

Celli, G.B., and de Lange, T. (2005). DNA processing is not required for ATM-mediated telomere damage response after TRF2 deletion. Nat. Cell Biol. *7*, 712–718.

Chiang, Y.J., Kim, S.H., Tessarollo, L., Campisi, J., and Hodes, R.J. (2004). Telomere-associated protein TIN2 is essential for early embryonic development through a telomerase-independent pathway. Mol. Cell. Biol. *24*, 6631–6634.

Chida, D., Nakagawa, S., Nagai, S., Sagara, H., Katsumata, H., Imaki, T., Suzuki, H., Mitani, F., Ogishima, T., Shimizu, C., et al. (2007). Melanocortin 2 receptor is required for adrenal gland development, steroidogenesis, and neonatal gluconeogenesis. Proc. Natl. Acad. Sci. USA *104*, 18205–18210.

Chin, K., de Solorzano, C.O., Knowles, D., Jones, A., Chou, W., Rodriguez, E.G., Kuo, W.L., Ljung, B.M., Chew, K., Myambo, K., et al. (2004). In situ analyses of genome instability in breast cancer. Nat. Genet. *36*, 984–988.

Chin, L., Artandi, S.E., Shen, Q., Tam, A., Lee, S.L., Gottlieb, G.J., Greider, C.W., and DePinho, R.A. (1999). p53 deficiency rescues the adverse effects of telomere loss and cooperates with telomere dysfunction to accelerate carcinogenesis. Cell *97*, 527–538.

Choi, J., Southworth, L.K., Sarin, K.Y., Venteicher, A.S., Ma, W., Chang, W., Cheung, P., Jun, S., Artandi, M.K., Shah, N., et al. (2008). TERT promotes epithelial proliferation through transcriptional control of a Myc- and Wnt-related developmental program. PLoS Genet. *4*, e10.

Cosme-Blanco, W., Shen, M.F., Lazar, A.J., Pathak, S., Lozano, G., Multani, A.S., and Chang, S. (2007). Telomere dysfunction suppresses spontaneous tumorigenesis in vivo by initiating p53-dependent cellular senescence. EMBO Rep. *8*, 497–503.

Cui, R., Widlund, H.R., Feige, E., Lin, J.Y., Wilensky, D.L., Igras, V.E., D'Orazio, J., Fung, C.Y., Schanbacher, C.F., Granter, S.R., and Fisher, D.E. (2007). Central role of p53 in the suntan response and pathologic hyperpigmentation. Cell *128*, 853–864.

de Lange, T. (2005). Shelterin: the protein complex that shapes and safeguards human telomeres. Genes Dev. *19*, 2100–2110.

Donehower, L.A., Harvey, M., Slagle, B.L., McArthur, M.J., Montgomery, C.A., Jr., Butel, J.S., and Bradley, A. (1992). Mice deficient for p53 are developmentally normal but susceptible to spontaneous tumours. Nature *356*, 215–221.

Else, T., and Hammer, G.D. (2005). Genetic analysis of adrenal absence: agenesis and aplasia. Trends Endocrinol. Metab. *16*, 458–468.

Else, T., Theisen, B.K., Wu, Y., Hutz, J.E., Keegan, C.E., Hammer, G.D., and Ferguson, D.O. (2007). Tpp1/Acd maintains genomic stability through a complex role in telomere protection. Chromosome Res. *15*, 1001–1013.

Else, T., Giordano, T.J., and Hammer, G.D. (2008). Evaluation of telomere length maintenance mechanisms in adrenocortical carcinoma. J. Clin. Endocrinol. Metab. *93*, 1442–1449.

Enders, G.C., and May, J.J., 2nd. (1994). Developmentally regulated expression of a mouse germ cell nuclear antigen examined from embryonic day 11 to adult in male and female mice. Dev. Biol. *163*, 331–340.

Farazi, P.A., Glickman, J., Jiang, S., Yu, A., Rudolph, K.L., and DePinho, R.A. (2003). Differential impact of telomere dysfunction on initiation and progression of hepatocellular carcinoma. Cancer Res. *63*, 5021–5027.

Feig, C., Kirchhoff, C., Ivell, R., Naether, O., Schulze, W., and Spiess, A.N. (2007). A new paradigm for profiling testicular gene expression during normal and disturbed human spermatogenesis. Mol. Hum. Reprod. *13*, 33–43.

Greider, C.W. (1996). Telomere length regulation. Annu. Rev. Biochem. *65*, 337–365.

Guo, X., Deng, Y., Lin, Y., Cosme-Blanco, W., Chan, S., He, H., Yuan, G., Brown, E.J., and Chang, S. (2007). Dysfunctional telomeres activate an ATM-ATR-dependent DNA damage response to suppress tumorigenesis. EMBO J. *26*, 4709–4719.

Hadshiew, I., Barre, K., Bodo, E., Funk, W., and Paus, R. (2008). T-oligos as differential modulators of human scalp hair growth and pigmentation: a new "time lapse system" for studying human skin and hair follicle biology in vitro? Arch. Dermatol. Res. *300*, 155–159.

Hande, M.P., Samper, E., Lansdorp, P., and Blasco, M.A. (1999). Telomere length dynamics and chromosomal instability in cells derived from telomerase null mice. J. Cell Biol. *144*, 589–601.

Hemann, M.T., and Greider, C.W. (2000). Wild-derived inbred mouse strains have short telomeres. Nucleic Acids Res. *28*, 4474–4478.

Hemann, M.T., Rudolph, K.L., Strong, M.A., DePinho, R.A., Chin, L., and Greider, C.W. (2001). Telomere dysfunction triggers developmentally regulated germ cell apoptosis. Mol. Biol. Cell *12*, 2023–2030.

Hockemeyer, D., Daniels, J.P., Takai, H., and de Lange, T. (2006). Recent expansion of the telomeric complex in rodents: Two distinct POT1 proteins protect mouse telomeres. Cell *126*, 63–77.

Hockemeyer, D., Palm, W., Else, T., Daniels, J.P., Takai, K.K., Ye, J.Z., Keegan, C.E., de Lange, T., and Hammer, G.D. (2007). Telomere protection by mammalian Pot1 requires interaction with Tpp1. Nat. Struct. Mol. Biol. *14*, 754–761.

Houghtaling, B.R., Cuttonaro, L., Chang, W., and Smith, S. (2004). A dynamic molecular link between the telomere length regulator TRF1 and the chromosome end protector TRF2. Curr. Biol. *14*, 1621–1631.

Jacks, T., Remington, L., Williams, B.O., Schmitt, E.M., Halachmi, S., Bronson, R.T., and Weinberg, R.A. (1994). Tumor spectrum analysis in p53-mutant mice. Curr. Biol. *4*, 1–7.

Jacobs, J.J., and de Lange, T. (2004). Significant role for p16INK4a in p53-independent telomere-directed senescence. Curr. Biol. *14*, 2302–2308.

Ju, Z., and Rudolph, K.L. (2006). Telomeres and telomerase in cancer stem cells. Eur. J. Cancer *42*, 1197–1203.

Karlseder, J., Kachatrian, L., Takai, H., Mercer, K., Hingorani, S., Jacks, T., and de Lange, T. (2003). Targeted deletion reveals an essential function for the telomere length regulator Trf1. Mol. Cell. Biol. *23*, 6533–6541.

Keegan, C.E., Hutz, J.E., Else, T., Adamska, M., Shah, S.P., Kent, A.E., Howes, J.M., Beamer, W.G., and Hammer, G.D. (2005). Urogenital and caudal dysgenesis in adrenocortical dysplasia (acd) mice is caused by a splicing mutation in a novel telomeric regulator. Hum. Mol. Genet. *14*, 113–123.

Khlgatian, M.K., Hadshiew, I.M., Asawanonda, P., Yaar, M., Eller, M.S., Fujita, M., Norris, D.A., and Gilchrest, B.A. (2002). Tyrosinase gene expression is regulated by p53. J. Invest. Dermatol. *118*, 126–132.

Kim, J., Chu, J., Shen, X., Wang, J., and Orkin, S.H. (2008). An extended transcriptional network for pluripotency of embryonic stem cells. Cell *132*, 1049–1061.

Lee, H.W., Blasco, M.A., Gottlieb, G.J., Horner, J.W., II, Greider, C.W., and DePinho, R.A. (1998). Essential role of mouse telomerase in highly proliferative organs. Nature *392*, 569–574.

Liu, D., Safari, A., O'Connor, M.S., Chan, D.W., Laegeler, A., Qin, J., and Songyang, Z. (2004). PTOP interacts with POT1 and regulates its localization to telomeres. Nat. Cell Biol. *6*, 673–680.

Liu, Y., Snow, B.E., Hande, M.P., Yeung, D., Erdmann, N.J., Wakeham, A., Itie, A., Siderovski, D.P., Lansdorp, P.M., Robinson, M.O., and Harrington, L. (2000). The telomerase reverse transcriptase is limiting and necessary for telomerase function in vivo. Curr. Biol. *10*, 1459–1462.

Luo, X., Ikeda, Y., Lala, D.S., Baity, L.A., Meade, J.C., and Parker, K.L. (1995). A cell-specific nuclear receptor plays essential roles in adrenal and gonadal development. Endocr. Res. *21*, 517–524.

Maser, R.S., and DePinho, R.A. (2002). Connecting chromosomes, crisis, and cancer. Science *297*, 565–569.

Meeker, A.K., Gage, W.R., Hicks, J.L., Simon, I., Coffman, J.R., Platz, E.A., March, G.E., and De Marzo, A.M. (2002). Telomere length assessment in human archival tissues: combined telomere fluorescence in situ hybridization and immunostaining. Am. J. Pathol. *160*, 1259–1268.

Mendiola, M., Carrillo, J., Garcia, E., Lalli, E., Hernandez, T., de Alava, E., Tirode, F., Delattre, O., Garcia-Miguel, P., Lopez-Barea, F., et al. (2006). The orphan nuclear receptor DAX1 is up-regulated by the EWS/FLI1 oncoprotein and is highly expressed in Ewing tumors. Int. J. Cancer *118*, 1381–1389.

Niakan, K.K., Davis, E.C., Clipsham, R.C., Jiang, M., Dehart, D.B., Sulik, K.K., and McCabe, E.R. (2006). Novel role for the orphan nuclear receptor Dax1 in embryogenesis, different from steroidogenesis. Mol. Genet. Metab. *88*, 261–271.

O'Connor, M.S., Safari, A., Xin, H., Liu, D., and Songyang, Z. (2006). A critical role for TPP1 and TIN2 interaction in high-order telomeric complex assembly. Proc. Natl. Acad. Sci. USA *103*, 11874–11879.

O'Hagan, R.C., Chang, S., Maser, R.S., Mohan, R., Artandi, S.E., Chin, L., and DePinho, R.A. (2002). Telomere dysfunction provokes regional amplification and deletion in cancer genomes. Cancer Cell *2*, 149–155.

Poncet, D., Belleville, A., de Roodenbeke, C.T., de Climens, A.R., Simon, E.B., Merle-Beral, H., Callet-Bauchu, E., Salles, G., Sabatier, L., Delic, J., and Gilson, E. (2008). Changes in the expression of telomere maintenance genes suggest global telomere dysfunction in B-chronic lymphocytic leukemia. Blood *111*, 2388–2391.

Rudolph, K.L., Chang, S., Lee, H.W., Blasco, M., Gottlieb, G.J., Greider, C., and DePinho, R.A. (1999). Longevity, stress response, and cancer in aging telomerase-deficient mice. Cell *96*, 701–712.

Rudolph, K.L., Millard, M., Bosenberg, M.W., and DePinho, R.A. (2001). Telomere dysfunction and evolution of intestinal carcinoma in mice and humans. Nat. Genet. *28*, 155–159.

Sarin, K.Y., Cheung, P., Gilison, D., Lee, E., Tennen, R.I., Wang, E., Artandi, M.K., Oro, A.E., and Artandi, S.E. (2005). Conditional telomerase induction causes proliferation of hair follicle stem cells. Nature *436*, 1048–1052.

Schrader, M., Muller, M., Schulze, W., Heicappell, R., Krause, H., Straub, B., and Miller, K. (2002). Quantification of telomerase activity, porphobilinogen deaminase and human telomerase reverse transcriptase mRNA in testicular tissue—new parameters for a molecular diagnostic classification of spermatogenesis disorders. Int. J. Androl. *25*, 34–44.

Smogorzewska, A., and de Lange, T. (2002). Different telomere damage signaling pathways in human and mouse cells. EMBO J. *21*, 4338–4348.

Tabori, U., Nanda, S., Druker, H., Lees, J., and Malkin, D. (2007). Younger age of cancer initiation is associated with shorter telomere length in Li-Fraumeni syndrome. Cancer Res. *67*, 1415–1418.

van Steensel, B., Smogorzewska, A., and de Lange, T. (1998). TRF2 protects human telomeres from end-to-end fusions. Cell *92*, 401–413.

Vega, F., Cho-Vega, J.H., Lennon, P.A., Luthra, M.G., Bailey, J., Breeden, M., Jones, D., Medeiros, L.J., and Luthra, R. (2008). Splenic marginal zone lymphomas are characterized by loss of interstitial regions of chromosome 7q, 7q31.32 and 7q36.2 that include the protection of telomere 1 (POT1) and sonic hedgehog (SHH) genes. Br. J. Haematol. *142*, 216–226.

Wu, L., Multani, A.S., He, H., Cosme-Blanco, W., Deng, Y., Deng, J.M., Bachilo, O., Pathak, S., Tahara, H., Bailey, S.M., et al. (2006). Pot1 deficiency initiates DNA damage checkpoint activation and aberrant homologous recombination at telomeres. Cell *126*, 49–62.

Xin, H., Liu, D., Wan, M., Safari, A., Kim, H., Sun, W., O'Connor, M.S., and Songyang, Z. (2007). TPP1 is a homologue of ciliate TEBP-beta and interacts with POT1 to recruit telomerase. Nature *445*, 559–562.

Ye, J.Z., Hockemeyer, D., Krutchinsky, A.N., Loayza, D., Hooper, S.M., Chait, B.T., and de Lange, T. (2004). POT1-interacting protein PIP1: a telomere length regulator that recruits POT1 to the TIN2/TRF1 complex. Genes Dev. *18*, 1649–1654.

Zanaria, E., Muscatelli, F., Bardoni, B., Strom, T.M., Guioli, S., Guo, W., Lalli, E., Moser, C., Walker, A.P., McCabe, E.R., et al. (1994). An unusual member of the nuclear hormone receptor superfamily responsible for X-linked adrenal hypoplasia congenita. Nature *372*, 635–641.